Supporting Information

Ultrathin CuO nanorods: controllable synthesis and superior catalytic properties in styrene epoxidation

Wei Jia[1], Yuxi Liu[1], Pengfei Hu[2], Rong Yu[3], Yu Wang[1], Lei Ma[1], Dingsheng Wang[1]* and

Yadong Li[1]

[1]Department of Chemistry and Collaborative Innovation Center for Nanomaterial Science and Engineering, Tsinghua University, Beijing, 100084 (P. R. China)
[2]Laboratory for Microstructures, Shanghai University, Shanghai 200444 (P. R. China)
[3]Department of Materials Science and Engineering, Tsinghua University, Beijing 100084 (P. R. China)
*E-mail: wangdingsheng@mail.tsinghua.edu.cn

Experimental details

Reagents: Reagents including CuCl, ethanol and cyclohexane were of analytical grade from the Beijing Chemical Factory of China. Oleylamine (80%-90%) was purchased from Acros. All the chemicals were used without further purification.

Synthesis of ultrathin CuO nanorods: In a standard synthesis of ultrathin CuO nanorods, 15 mg of CuCl was dissolved in 2 ml of oleylamine in a 5-mL vial. After the vial had been capped, the vial was transferred into an oil bath and magnetically stirred at 120 °C until CuCl was completely dissolved in oleylamine. Then open the cap and heated at 120 °C under magnetic stirring until the solution turned to dark brown. The collected products were rinsed with ethanol and cyclohexane for several times. Eventually the precipitates were redispersed in cyclohexane for further use. CuO nanoellipsoids and CuO nanoleaves were synthesized under similar reaction conditions except that the temperature used was 80 °C and 100 °C, respectively.

Synthesis of Cu nanowires: In a typical synthesis of copper nanowires, 51 mg of CuCl was uniformly put at the bottom of 5-ml vial, then 3 ml of oleylamine was cautiously added into the vial through a pipettor. After that they were transferred into an oil bath and kept at 200 °C for 12 h without magnetic stirring. The resulting reddish brown solution was centrifuged (6000 rpm for 8 min) and then washed with cyclohexane and ethanol several times. The products were redispersed in cyclohexane to avoid the oxidation of the copper nanowires.

Catalytic tests: The epoxidation of styrene was performed in a 50 mL two-necked round bottom flask equipped with a reflux condenser. Typically, 0.1 g as-prepared catalysts (CuO nanocrystals loaded onto MgAl-Layered double hydroxide (CuO/LDH), the Cu loading, measured by ICP, was 3.5 wt%, 3.2 wt% and 3.6 wt% for CuO-NRs/LDH, CuO-NLs/LDH and CuO-NEs/LDH, respectively.) and 10 mmol styrene were added to 15 mL acetonitrile and refluxed at 75 °C for 0.5 h under stirring. The catalytic reaction was initiated by adding 30 mmol tert-butylhydroperoxide (TBHP) to the mixture in the flask, then carried out with

vigorous stirring for 10 h. Resulting product mixtures were analysed by gas chromatography using tetradecane as an internal standard. Product identification and gas chromatograph calibration were carried out using both gas chromatography–mass spectroscopy and standard solutions of each product identified. Recycling reactions of CuO-NRs/LDH catalyst was tested by separating it from the reaction system by centrifugation, washing with large quantity of ethanol, and drying at 60 °C for 12 h, then the catalyst was reused in the next run under the same reaction conditions.

Characterization:

The crystallographic structure of the products was determined using a Rigaku RU-200b X-ray powder diffractometer with CuKα radiation (λ = 1.5418 Å). The morphologies of the products were examined with scanning electron microscopy (SEM, JEOL JSM-6301F), transmission electron microscopy (TEM, Hitachi-7700) and high-resolution transmission electron microscopy (HRTEM, FEI Tecnai G2 F20 S-Twin, operating at 200 kV). Additionally, the composition of the products was measured by inductively coupled plasma atomic emission spectroscopy (ICP-AES) and energy dispersive X-ray spectroscopy (EDX). X-ray photoelectron spectroscopy (XPS) experiments were performed on PHI-5300 Quantera microprobe. All binding energies were referred to the C 1s peak (284.7 eV).

The reactant conversion, product selectivity, and product yield were calculated as follows:

$$conversion\ (\%) = \frac{moles\ of\ reactant\ converted}{moles\ of\ reactant\ in\ feed} \times 100$$

$$product\ selectivity(\%) = \frac{moles\ of\ product\ formed}{moles\ of\ reactant\ converted} \times 100$$

$$product\ yield(\%) = \frac{conversion(\%) \times product\ selectivity(\%)}{100}$$

Supplementary Figures
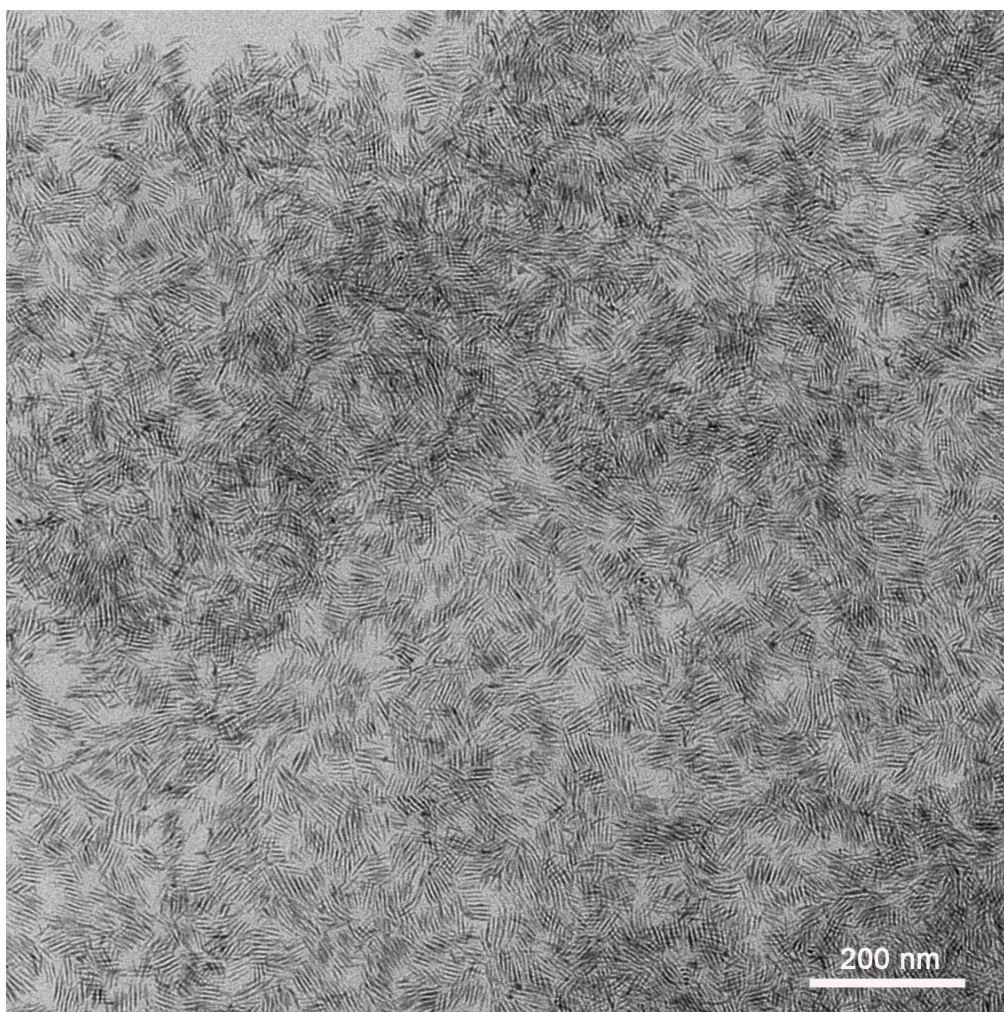
Figure S1. A large-area TEM image of the as-synthesized CuO nanorods.
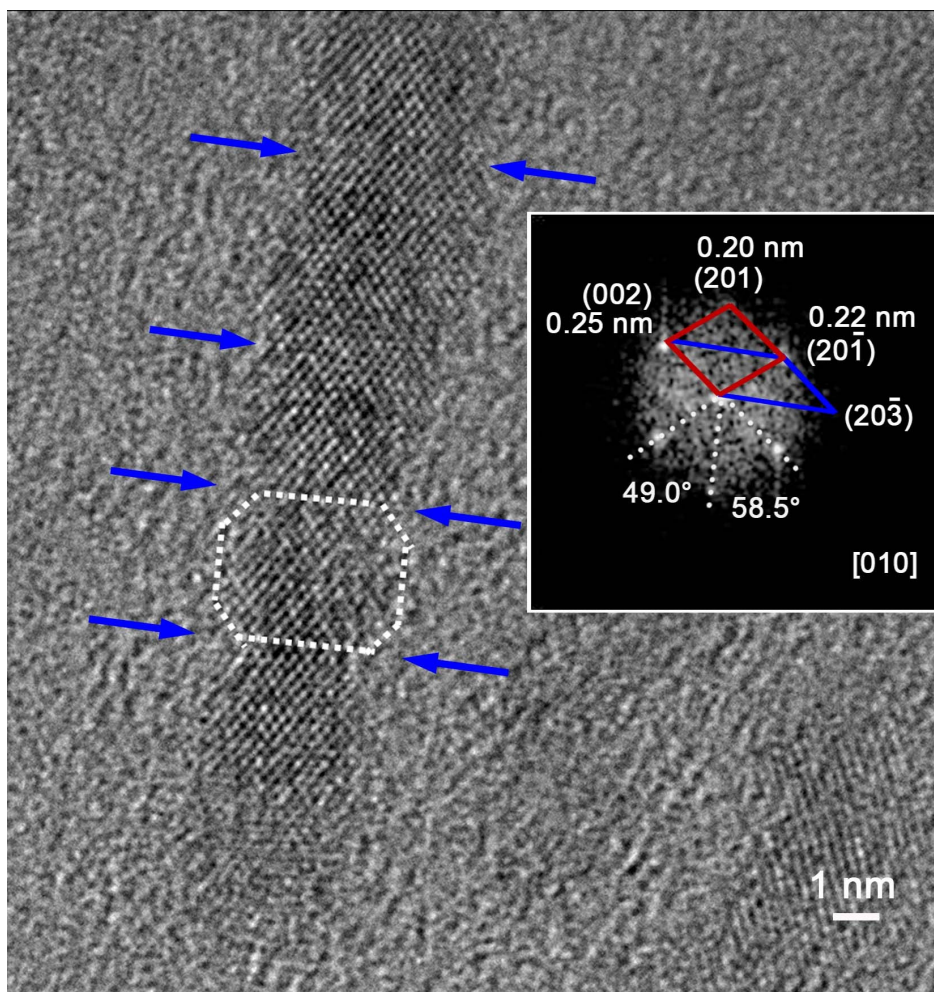
Figure S2. Typical HRTEM image of another individual nanorod projected from the [010] direction. The blue arrows indicate the necking sites. Inset is the FFT pattern.
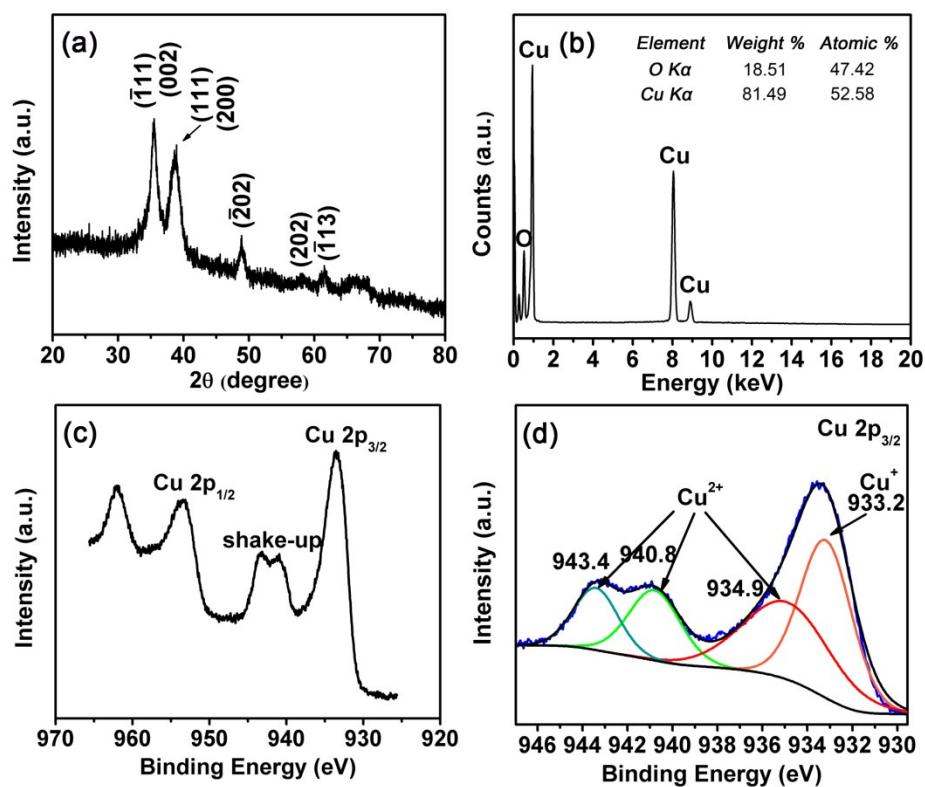
Figure S3. (a) XRD patterns of the as-prepared product; (b) EDX spectra reveals that the product is composed of Cu and O with a ratio of 1:1.1; (c) and (d) XPS characterization of the CuO nanostructures.

The surface of the as-obtained CuO sample was also investigated by XPS. As shown in Fig. 1c and d, the main peak at 933.5 eV belongs to Cu $2p_{3/2}$ is fitted into two peaks at 933.2 and 934.9 eV corresponding to Cu^0/Cu^+ and Cu^{2+}, respectively.[1] Additionally, the presence of shake-up satellites characterizing an open $3d^9$ shell, corresponding to Cu^{2+} state,[2] are also found in Fig. 1d. The presence of Cu_2O, not revealed by XRD, might be due to the reduction of Cu^{2+} under X-ray irradiation in the ultrahigh vacuum environment.[3]
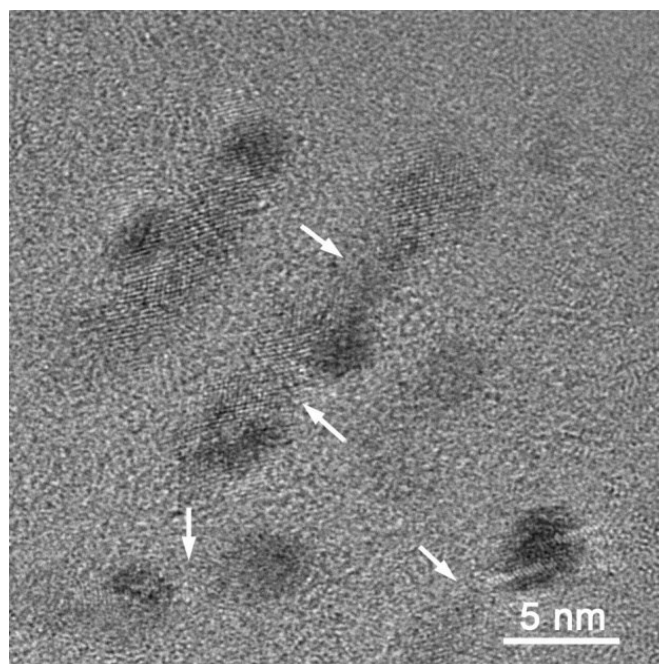
Figure S4. TEM image showing that the ultrathin CuO nanorods broke when exposed to electron beam with an accelerating voltage of 200 kV. The indicated arrows in the image exhibited the nanorods were breaking down into fragments.
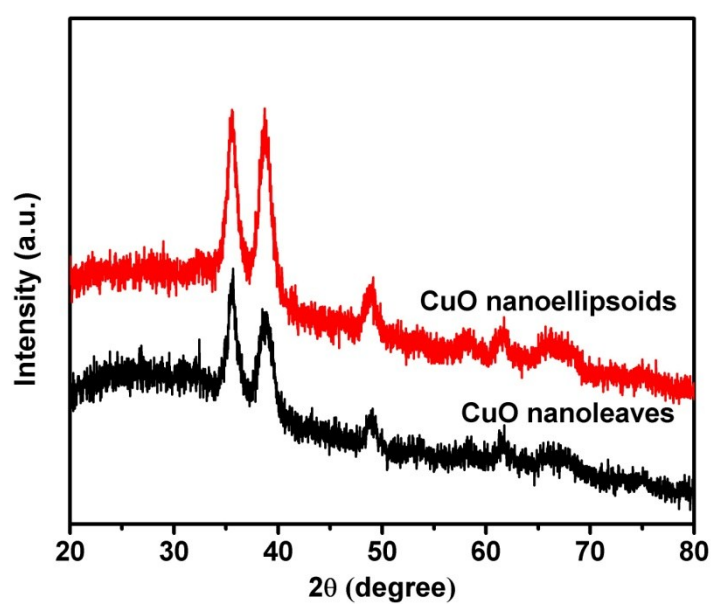
Figure S5. XRD patterns of CuO nanoellipsoids and nanoleaves obtained at 80 ºC and 100 ºC, respectively.
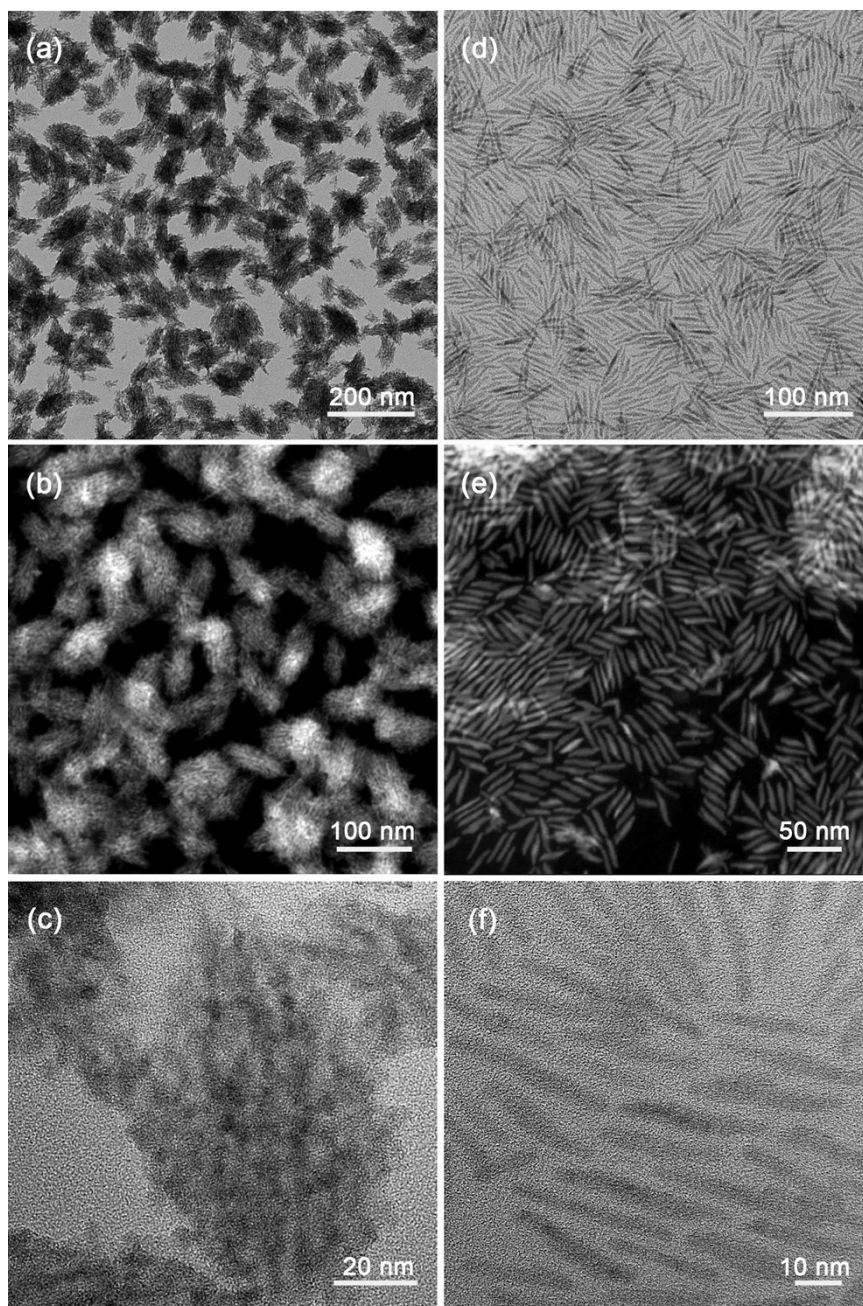
Figure S6. TEM images of CuO nanostructures formed at 80 °C (a-c) and 100 °C (d-f): (a, d) Bright-field TEM images; (b, e) HAADF-STEM images; (c, f) High-magnification TEM images.
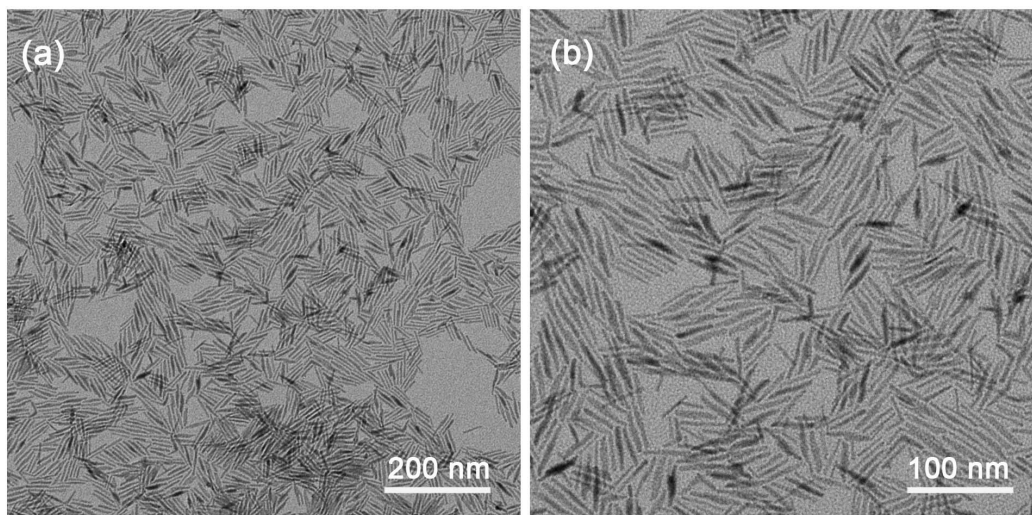
Figure S7. TEM images of the products obtained at 110 °C.
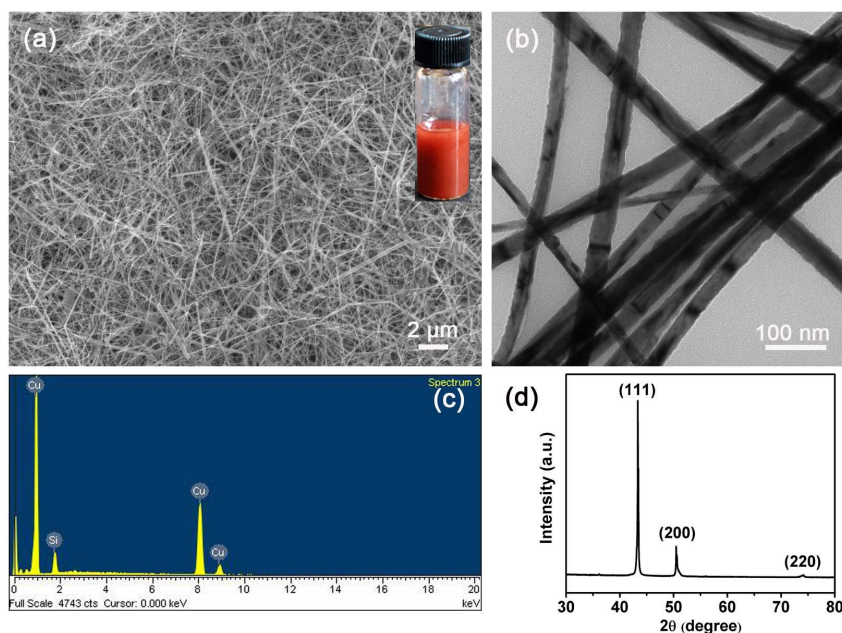
Figure S8. Cu nanowires synthesized by heating CuCl with oleylamine at 200 °C for 12 h: (a) SEM image; (b) TEM image; (c) EDX spectrum and (d) XRD pattern of Cu nanowires. The inset in (a) shows a photograph of the as-prepared suspension of Cu nanowires in cyclohexane.

The morphology of the as-prepared products was examined by SEM and TEM. The SEM and TEM images (Figure S8a, b) demonstrated that the final products are composed of a large quantity of nanowires with constant diameters in the range of 20-40 nm, and it has a typical length of several tens of micrometers. Figure S8d depicts the XRD pattern of the products. Cu nanowires were identified on the basis of the three clearly distinguishable diffraction peaks at 2θ = 43.3°, 50.4°, and 74.2° corresponding to the (111), (200) and (220) crystal planes of face-centered cubic (fcc) Cu (JCPDS file No. 04-0836), respectively. The chemical

composition of the nanowires was further confirmed by EDX spectroscopy (Figure S8c). A typical EDX spectrum shows presence of the Cu Kα line confirms the formation of Cu, whereas the Si signal originates from the Si substrate. The inset of Figure S8a also indicates the characteristic color of metallic Cu.
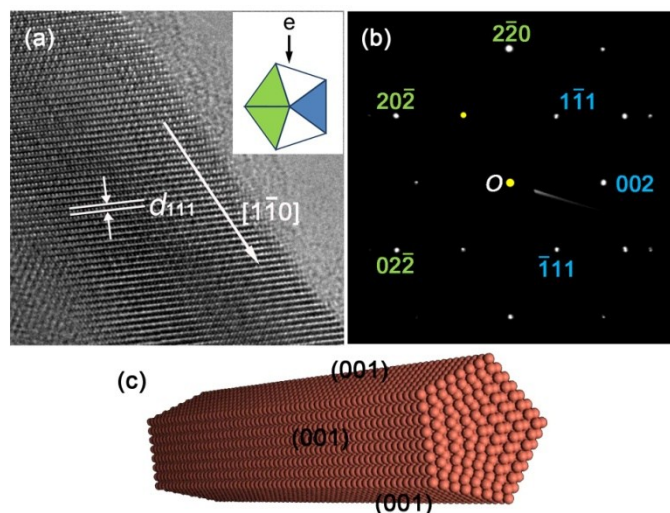
Figure S9. Structural characterizations of a Cu nanowire: (a) High-resolution TEM image of a single nanowire, showing $[1\bar{1}0]$ growth direction. (b) Diffraction pattern of a Cu nanowire viewed normal to the major axis. It may be indexed as the [111] and [110] zone axes of Cu. The yellow spots denote the reflections that were blocked by the beam blanker when recording the diffraction pattern. (c) Atomic model of a Cu nanowire. The inset in (a) shows a schematic cross-section of the five-fold twinned nanowire.

The structure characterization of individual nanowire was investigated in detail by HRTEM and SAED. Figure S9a shows the HRTEM image of an individual Cu nanowire with well-resolved (111) lattice fringes having a spacing of 0.21 nm. The corresponding SAED pattern with the electron beam direction normal to the major axis is shown in Figure S9b. As schematically shown in the inset of Figure S9a, when viewed in the direction labeled by the arrow, the two green sections give the diffraction spots in the [111] zone axis, and the blue section the [110] zone axis. The two sets of diffraction patterns share the same $(2\bar{2}0)$ reflection, which corresponds to the growth direction $[1\bar{1}0]$ for all the five sections. Based on the above analyses, we can conclude that the Cu nanowires have a five-fold twinned structure bounded by ten {111} faces at the two ends and five {100} side faces (Figure S9c), which is consistent with previous reports.[4]
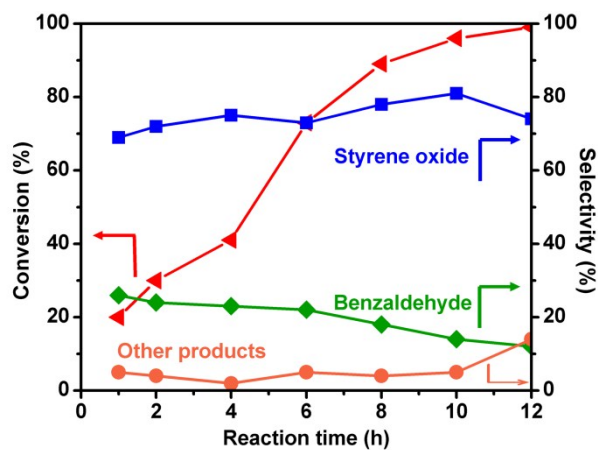
Figure S10. Influence of reaction time on the conversion and product selectivity in the epoxidation of styrene over CuO-NRs/LDH catalyst.

(reaction conditions: reaction mixture = 10 mmol styrene + 30 mmol TBHP + 0.1 g catalyst and bath temperature = 75 °C).
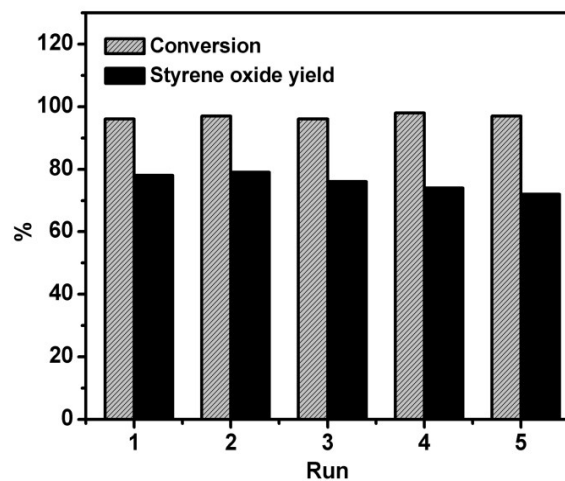
Figure S11. Recovery and reusability of the CuO-NRs/LDH as catalyst for the oxidation of styrene to styrene oxide.

(reaction conditions: reaction mixture = 10 mmol styrene + 30 mmol TBHP + 0.1 g catalyst and bath temperature = 75 °C).

Table S1

Comparison of the CuO/LDH catalysts with the earlier reported heterogeneous catalysts for their performance in the styrene-to-styrene oxide epoxidation.

Catalyst	Oxidizing agent used	Conversion (%)	Yield (%)	Ref.
TS-1	Urea-H_2O_2 adduct	71	61.8	[5]
Au/Yb_2O_3	TBHP (anhy.)	63.5	34.8	[6]
Au-PMO-SBA-15	TBHP (anhy.)	94.8	71.1	[7]
Pt@Fe_2O_3 nanowires	TBHP	33.9	27.4	[8]
$Pd_{0.3}Cu_{0.7}$	TBHP (aq.)	75	52.5	[9]
NiO/SiO_2	TBHP (aq.)	48.8	37.9	[10]
CuO CNCs@meso-SiO_2 nanocomposite	TBHP	88.6	54.2	[11]
CuO/In_2O_3	TBHP (anhy.)	65.2	48.1	[12]
CuO/Ga_2O_3	TBHP (aq.)	73.6	57.5	[12]
CuO-NEs/LDH	TBHP (aq.)	95.4	64.6	This work
CuO-NLs/LDH	TBHP (aq.)	98.1	75.5	This work
CuO-NRs/LDH	TBHP (aq.)	96.2	77.8	This work

It can be seen from Table S1, CuO-NRs/LDH catalyst shows better performance as compared to all the present and earlier catalysts. Compared to the metal oxide-supported CuO CNCs@meso-SiO_2 nanocomposite,[11] CuO/In_2O_3,[12] CuO/Ga_2O_3[12] and NiO/SiO_2[10] catalysts, our CuO/LDH catalysts display an enhanced conversion of styrene and higher yields of styrene oxide. Notably, the as-prepared CuO-NRs/LDH and CuO-NLs/LDH catalysts are not inferior to some supported nano-gold catalysts,[6-7] TS-1 catalyst[5] and alloy catalyst.[9]

References

1   J. P. Espinós, J. Morales, A. Barranco, A. Caballero, J. P. Holgado and A. R. González-Elipe, *J. Phys. Chem. B*, 2002, **106**, 6921.

2   J. Ghijsen, L. H. Tjeng, J. van Elp, H. Eskes, J. Westerink, G. A. Sawatzky and M. T. Czyzyk, *Phys. Rev. B*, 1988, **38**, 11322.

3   C.-K. Wu, M. Yin, S. O'Brien and J. T. Koberstein, *Chem. Mater.*, 2006, **18**, 6054; X.-Y. Yu, R.-X. Xu, C. Gao, T. Luo, Y. Jia, J.-H. Liu and X.-J. Huang, *ACS Appl. Mater. Interfaces*, 2012, **4**, 1954.

4   E. Ye, S.-Y. Zhang, S. Liu and M.-Y. Han, *Chem. Eur. J.*, 2011, **17**, 3074; H.-J. Yang, S.-Y. He and H.-Y. Tuan, *Langmuir*, 2014, **30**, 602.

5   S. C. Laha and R. Kumar, *J. Catal.*, 2001, **204**, 64.

6   V. R. Choudhary, D. K. Dumbre, N. S. Patil, B. S. Uphade and S. K. Bhargava, *J. Catal.*, 2013, **300**, 217.

7   Y. Jin, P. Wang, D. Yin, J. Liu, H. Qiu and N. Yu, *Micropor. Mesopor. Mater.*, 2008, **111**, 569.

8   H. Hong, L. Hu, M. Li, J. Zheng, X. Sun, X. Lu, X. Cao, J. Lu and H. Gu, *Chem. Eur. J.*, 2011, **17**, 8726.

9   J. Mao, Y. Liu, Z. Chen, D. Wang and Y. Li, *Chem. Commun.*, 2014, **50**, 4588.

10   V. R. Choudhary, R. Jha and P. Jana, *Catal. Commun.*, 2008, **10**, 205.

11   C. Chen, J. Qu, C. Cao, F. Niu and W. Song, *J. Mater. Chem.*, 2011, **21**, 774.

12   V. R. Choudhary, R. Jha, N. K. Chaudhari and P. Jana, *Catal. Commun.*, 2007, **8**, 1556.